Phenomenology of the Growth of Single-Walled Aluminosilicate and Aluminogermanate Nanotubes of Precise Dimensions

Sanjoy Mukherjee, Veda M. Bartlow, and Sankar Nair*

School of Chemical & Biomolecular Engineering, Georgia Institute of Technology, Atlanta, Georgia 30332-0100

Received March 15, 2005. Revised Manuscript Received June 15, 2005

We report a detailed phenomenological study of the growth and structural properties of single-walled aluminosilicate and aluminogermanate nanotubes with a structure analogous to the naturally occurring nanotube mineral imogolite. The evolution of the aqueous-phase nanotube synthesis process over a period of 5 days was carefully analyzed by a number of qualitative and quantitative characterization tools. In particular, the time-dependence of the nanotube size, structure, and solid-state packing was followed using electron microscopy, electron diffraction, X-ray diffraction, and dynamic light scattering. From analysis of the dispersed and solid-state properties of the nanotubes, we obtained several findings: (1) the dimensions of the aluminogermanate nanotubes are approximately 15 nm in length and 3.3 nm in their (outer) diameter, whereas those of the aluminosilicate nanotubes are 100 and 2.2 nm, respectively; (2) nanotube materials are formed at a very early stage in the reaction; (3) the structure of the nanotubes remains essentially identical throughout the synthesis though their concentration increases with synthesis time; (4) their solid-state packing is well-ordered in an apparently monoclinic (and not hexagonal) arrangement; and (5) their dimensions (both diameter and length) appear monodisperse. The essentially constant size and structure of the nanotubes over their entire synthesis time, the increasing nanotube concentration over the synthesis time, and the absence of significant polydispersity strongly suggest that these nanotubular inorganic macromolecules are assembled through a thermodynamically controlled self-assembly process rather than a kinetically controlled growth/polymerization process.

I. Introduction

Nanotubular materials[1] are important building blocks of a future nanotechnology based on synthesis of functional nanoparticles and their assembly into nanoscale devices with novel applications in areas such as electronics, biotechnology, sensing, separations, energy storage/management, and catalysis. The discovery of carbon nanotubes[2] has stimulated extensive research on the synthesis, properties, and applications of nanotubes, with the majority of the studies being focused on the novel properties of carbon nanotubes. However, several problems in carbon nanotube technology remain to be overcome, for example, the development of a low-temperature synthetic process with high yield as well as precise control over the nanotube dimensions and chirality, limitations of chemical composition, and the production of "three-dimensionally nanoscale" carbon nanotube objects (i.e., single-walled objects smaller than 10 nm in both length and cross section). To achieve their full potential, nanotechnological applications will ultimately require precise control over nanotube dimensions and monodispersity at length scales below 100 nm.

Inorganic nanotubes,[3] nanorods, and nanowires are being increasingly investigated for nanotechnological applications owing, among several factors, to the vast range of potential physicochemical properties afforded by inorganic materials. Several of these structures are synthesized using carbon nanotubes as templates, and thus, possess the same potential difficulty of controlling the nanoparticle dimensions. Most of the inorganic nanotubes synthesized to date, apart from molybdenum disulfide (MoS_2), are polydisperse and/or multiwalled materials.[3−6] In addition, they have high aspect ratios and are several hundred nanometers to micrometers in length. An apparent exception is the synthetic version of the naturally occurring nanotube mineral imogolite.[7] The synthesis and properties of these materials have been investigated to a significant extent over the years.[7−12] Imogolite is a single-walled nanotube (Figure 1a,b) whose wall structure is identical to a layer of aluminum(III) hydroxide (gibbsite), with isolated silicate groups bound on the inner wall. The nanotube has a periodic wall structure

* Corresponding author. E-mail: sankar.nair@chbe.gatech.edu.

(1) Lieber, C. M. *Solid State Commun.* **1998**, *107* (11), 607−616.
(2) Iijima, S. *Nature* **1991**, *354* (6348), 56−58.
(3) Rao, C. N. R.; Nath, M. *Dalton Trans.* **2003**, (*1*), 1−24.
(4) Patzke, G. R.; Krumeich, F.; Nesper, R. *Angew. Chem., Int. Ed.* **2002**, *41* (14), 2446−2461.
(5) Zhu, Y. Q.; Hsu, W. K.; Terrones, H.; Grobert, N.; Chang, B. H.; Terrones, M.; Wei, B. Q.; Kroto, H. W.; Walton, D. R. M.; Boothroyd, C. B.; Kinloch, I.; Chen, G. Z.; Windle, A. H.; Fray, D. J. *J. Mater. Chem.* **2000**, *10* (11), 2570−2577.
(6) Rosentsveig, R.; Margolin, A.; Feldman, Y.; Popovitz-Biro, R.; Tenne, R. *Chem. Mater.* **2002**, *14* (2), 471−473.
(7) Cradwick, P. D.; Wada, K.; Russell, J. D.; Yoshinaga, N.; Masson, C. R.; Farmer, V. C. *Nature (London), Phys. Sci.* **1972**, *240* (104), 187−198.
(8) Russel, J. D.; McHardy, W. J.; Fraser, A. R. *Clay Miner.* **1969**, *8*, 87−99.
(9) Wada, K.; Yoshinga, N. *Am. Mineral.* **1969**, *54* (1−2), 50−56
(10) Farmer, V. C.; Fraser, A. R.; Tait, J. M., *J. Chem. Soc., Chem. Commun.* **1977**, (*13*), 462−463.
(11) Farmer, V. C.; Smith, B. F. L.; Tait, J. M. *Clay Miner.* **1979**, *14* (2), 103−107.
(12) Wada, S. I.; Eto, A.; Wada, K. *J. Soil Sci.* **1979**, *30* (2), 347−352

10.1021/cm0505852 CCC: $30.25
Published on Web 09/03/2005

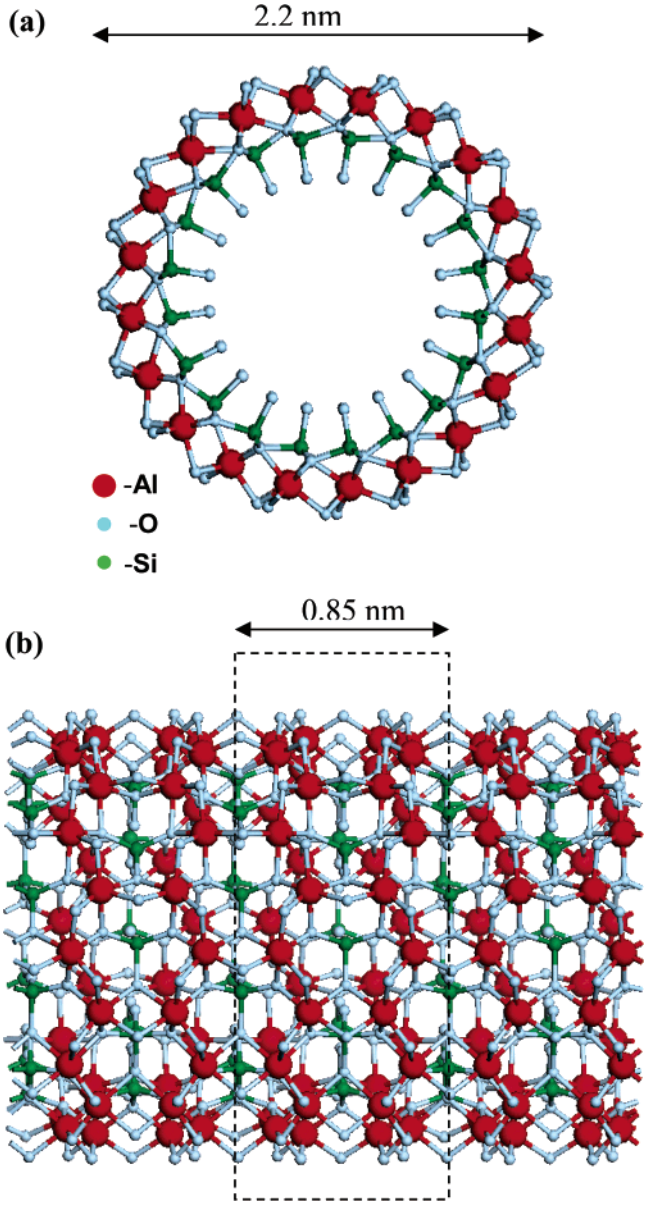

Figure 1. Structure of the aluminosilicate nanotube, imogolite. (a) Cross-sectional view showing the nanopore and (b) side view.

composed of six-membered aluminum hydroxide rings, with a repeat unit of approximately 0.85 nm along the nanotube axis.[7] The empirical formula of imogolite is $(OH)_3Al_2O_3$-SiOH. The presence of hydroxyl groups on walls and rims makes the nanotube hydrophilic. Naturally occurring imogolite has an external diameter of around 2.0 nm and an internal diameter of around 1.0 nm.[9] The structural model shown in Figure 1 was proposed[7−9] on the basis of solid-state NMR, transmission electron microscopy (TEM), and X-ray diffraction (XRD) studies that established its close relation to the layered structure of gibbsite as well as the coordination environment of the Al and Si atoms. Synthetic imogolite was prepared[10] from a millimolar aluminosilicate precursor solution at a temperature of 95 °C. The typical solid-state structure consists of nanotube bundles or ropes several micrometers in length. An aluminogermanate analogue has also been successfully prepared by substitution of silicon with germanium in the synthesis solution.[13] However, from the limited amount of characterization data available, the aluminogermanate (Al−Ge) analogues appear considerably shorter than the aluminosilicate (Al−Si) nanotubes, and their diameters are about 50% larger.

From the perspective of nanomaterials engineering, we are particularly interested in the potential nanotechnological applications of inorganic nanotubes with well-defined length and diameter that can be synthesized via relatively mild chemistry and which have technologically useful properties different from those of carbon nanotubes. Imogolite nanotubes have been investigated for use as a catalyst support[14,15] and for methane storage.[16] However, we are investigating other potential applications for these nanotubes. For example, the Al−Ge nanotubes, which are as short as 10 nm with an outside diameter of 3.3 nm (see Results and Discussion), are attractive candidates for use in artificial ion channel devices as a result of their well-defined solid-state structure, hydrophilic interior, and short length. Artificial ion channels have high potential for biomolecule sensing devices, particularly for high-speed DNA and protein analysis.[17] These devices operate by detecting chain biopolymers as they translocate through a nanoscale ion-conducting channel. The variation in the ion conductance of the channel, when correlated to the biopolymer properties, can lead to novel sensing strategies with single-molecule resolution and high speed. Intrinsic limitations on the stability and reliability of nanoscale ion channels made from "soft matter" such as proteins have led to a requirement for solid-state hydrophilic ion channels of appropriate length and diameter.[18] Similarly, others have proposed the construction of nanocomponents such as nanoelectrical cables (containing a conducting polymer wire with an insulating nanotube sheath) by the threading of polymers into short nanotubes. A number of recent simulation studies[19−21] using carbon nanotube models (<5 nm in length) have suggested the potential for the above applications. However, the synthesis of short, monodisperse nanotubes required for these applications is a difficult problem to tackle with current carbon nanotube technology.

Our investigations into the synthesis and properties of inorganic nanotubes indicate that imogolite Al−Si and Al−Ge nanotubes have unique properties (e.g., short length, hydrophilicity, ability to disperse in the aqueous phase, well-defined structure, and monodispersity) which make them attractive candidates for the above applications. Despite the potential nanotechnological applications of imogolite-like nanotubes, the phenomenology and mechanism of its formation are not well-understood. Previous investigators have

(13) Wada, S.; Wada, K. *Clays Clay Miner.* **1982**, *30* (2), 123−128.
(14) Imamura, S.; Kokubu, T.; Yamashita, T.; Okamoto, Y.; Kajiwara, K.; Kanai, H. *J. Catal.* **1996**, *160* (1), 137−139.
(15) Marzan, L. L.; Philipse, A. P. *Colloids Surf., A* **1994**, *90* (1), 95−109.
(16) Ohashi, F.; Tomura, S.; Akaku, K.; Hayashi, S.; Wada, S. I. *J. Mater. Sci.* **2004**, *39* (5), 1799−1801.
(17) Nakane, J. J.; Akeson, M.; Marziali, A. *J. Phys.: Condens. Matter* **2003**, *15* (32), R1365−R1393.
(18) Kong, C. Y.; Muthukumar, M. *Electrophoresis* **2002**, *23* (16), 2697−2703.
(19) Gao, H. J.; Kong, Y.; Cui, D. X.; Ozkan, C. S. *Nano Lett.* **2003**, *3* (4), 471−473.
(20) Kalra, A.; Garde, S.; Hummer, G. *Proc. Natl. Acad. Sci. U.S.A.* **2003**, *100* (18), 10175−10180.
(21) Hummer, G.; Rasaiah, J. C.; Noworyta, J. P. *Nature* **2001**, *414* (6860), 188−190.

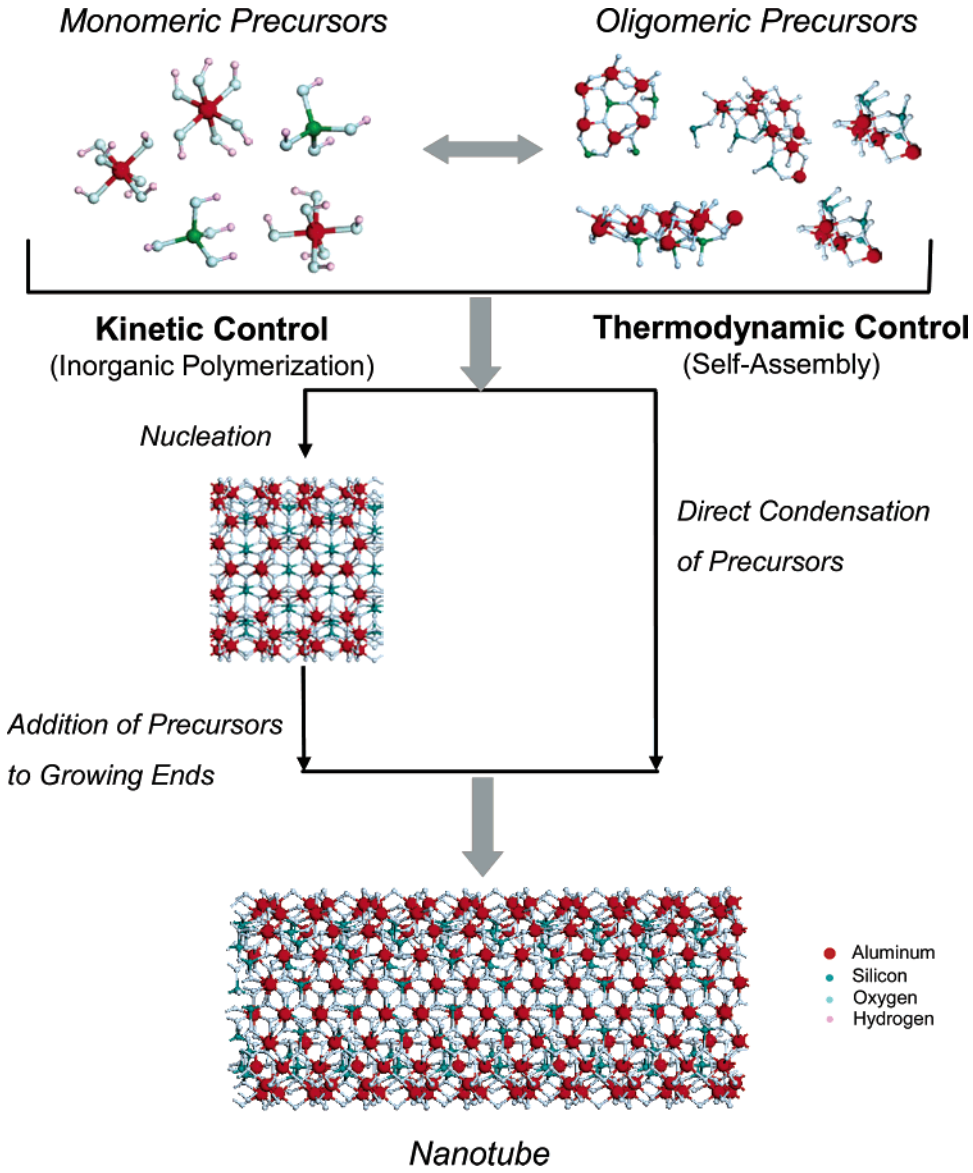

Figure 2. Schematic of possible mechanistic pathways leading to the formation of short aluminosilicate and aluminogermanate nanotubes in the aqueous phase.

suggested a mechanism based on the formation of sheets/layers of gibbsite which eventually develop curvature due to the binding of silicate groups. The curvature results from the differing bond lengths of the Al−O and Si−O bonds (0.19 and 0.16 nm, respectively); that is, the tetravalent silicon atoms pull the oxygen atoms in the aluminum hydroxide layer into a curved cylinder. The formation of imogolite has been proposed to occur from the intermediate "proto-imogolite", which is presumably a sheetlike particle.[11] However, its structure could not be detected by TEM, and its existence is proposed on the basis of the structure of imogolite. It was observed that the quantity of nanotubes seemed to grow substantially with the reaction time, with all the precursors being consumed by about 120 h of synthesis time.[22] Thus, it was suggested[22,23] that the formation of "proto-imogolite" precursors took place early in the reaction, and these precursors provided nuclei to the growth and formation of nanotubes by polymerization. However, definitive experimental proof of this mechanism is lacking. In contrast to this kinetically driven mechanism, a thermodynamically driven self-assembly process could also operate. Figure 2 shows a schematic of the main events that are likely to occur in the each of the two possible mechanisms. In a kinetically driven growth, the nanotube length would increase substantially with synthesis time as growth units are added to the end of the nanotube, whereas in a thermodynamically controlled self-assembly process, nanotubes of specific dimensions are expected to self-assemble as dictated by the precursor solution properties and the temperature. The two synthesis mechanisms, hence, require different approaches toward controlling the nanomaterial structure.

In the present paper, we report a systematic study of the growth of imogolite aluminosilicate and aluminogermanate nanotubes. Our approach is based on the use of a number of complementary characterization techniques to probe the dimensions, structure, and morphology of the nanotubes both

(22) Wilson, M. A.; Lee, G. S. H.; Taylor, R. C. *J. Non-Cryst. Solids* **2001**, *296* (3), 172−181.
(23) Bursill, L. A.; Peng, J. L.; Bourgeois, L. N. *Philos. Mag. A* **2000**, *80* (1), 105−117.

in the solid state and in the aqueous phase, as a function of synthesis time. In particular, samples withdrawn at specific times (up to 120 h) from the nanotube synthesis reactor are then characterized using TEM, selected area electron diffraction (SAED), XRD, and dynamic light scattering (DLS). TEM and XRD data were used to extract information on the morphology of the nanotubes and to propose a model for their packing in the solid state. SAED was used to ascertain the internal structure of the nanotubes as a function of growth time. Detailed mathematical analysis of DLS data provided quantitative information on the dimensions of the nanotubes in solution. The combination of characterization techniques revealed new aspects of the process of nanotube formation and structure, which are discussed below. The experimental evidence obtained in this paper is then discussed in the context of the two possible types of nanotube formation mechanisms. The phenomenology of aqueous-phase Al−Si and Al−Ge nanotube growth as developed here is a required step toward understanding the mechanisms of formation of these nanoscale materials and further using the insights gained to synthesize and apply new classes of functional nanomaterials.

II. Experimental Section

II.1. Synthesis. Tetraethyl orthosilicate (TEOS) was added dropwise to a stirred solution of 5 mM $AlCl_3$ solution until the Al:Si ratio was 1.8 and left to stand for 45 min under vigorous stirring. Then a 0.1 N NaOH solution was added at the rate of 0.3 mL/min until the pH of the solution reached 5.0. The pH was brought down immediately to 4.5 by dropwise addition of a solution containing 0.1 M HCl and 0.2 M acetic acid. The resulting clear solution was stirred for 3 h and then reacted at 95 °C under reflux conditions. A similar procedure was followed for the aluminogermanate NT, except that TEOS was substituted by $GeCl_4$. For DLS analysis, 5 mL of the sample was filtered through a 0.2 μm pore size syringe filter to produce a dust-free sample containing only nanoscale particles. A drop of the sample was deposited on a Formvar-backed copper TEM grid for electron microscopy and diffraction analysis. The remaining sample was transferred into a vessel under vigorous stirring. The 0.1 N ammonia solution was added carefully until the pH reached 8.0. At this point the solution turned murky and was centrifuged at 3000 rpm for 20 min. The supernatant was discarded, and the gel was acidified with a few drops of 12 N HCl. The resulting solution was immediately dialyzed against deionized water for 96 h to remove any unreacted precursors as well as sodium and chlorine ions. A total of 5 mL of dialyzed solution was evaporated over a glass slide to deposit a film of NTs amenable to XRD and XPS (X-ray photoelectron spectroscopy) analysis. A portion of the dialyzed sample was freeze-dried and used for nitrogen adsorption measurements.

II.2. Characterization. TEM images and SAED patterns were obtained with a JEOL JEM 100CX transmission electron microscope operated at 100 kV. As a result of the low contrast of the nanotubes, imaging was restricted to slight underfocus conditions. Because the converging electron beam tends to destroy the sample, the electron diffraction (ED) patterns were recorded first. A parallel, rather than convergent, electron beam was used to reduce electron dosage while obtaining the ED patterns. Thin-film XRD analysis was performed on a PAnalytical X'pert Pro diffractometer operating with a Cu Kα source and equipped with a diffracted beam collimator and a Miniprop detector. The data were collected in grazing angle incidence mode, with the incident beam at a fixed grazing angle of 1° with respect to the sample plane and the detector scanning over angles from 2 to 30° with respect to the same plane. The NT films were analyzed for surface composition with a PH1 model SCA 1600 XPS instrument equipped with a monochromatic Al Kα source (1486.4 eV) and a spherical capacitor analyzer operating at a 187.85 eV pass energy. High-resolution spectra (0.05 eV/step and 50 ms/step) were collected for bond information by peak deconvolution using Gauss−Lorentzian peaks. Nitrogen adsorption measurements were performed at 77 K using a Micrometrics ASAP 2000M adsorption analyzer. The samples were first outgassed for 12 h at 250 °C. A static volumetric method was used to obtain the volume of nitrogen adsorbed as a function of relative pressure in the range of 10^{-3} to 10^{0}. This was sufficient to scan the expected range of the nanotube pore size. The pore size distribution was determined using the Horvath−Kawazoe (HK)[24] model (developed for slit shaped pores) with the Saito−Foley[25] modification for cylindrical pores. DLS data were collected with a Protein Solutions DynaPro instrument. The scattering angle was 90°, and the laser wavelength was 720 nm. The autocorrelator delay time (τ) was 1 μs. At least 20 scans were performed on each sample, each with a 10 s acquisition time. Initial cumulant analysis[26] was used to discard uncharacteristic or erroneous scans affected by scattering from stray particles (e.g., dust) in the sample.

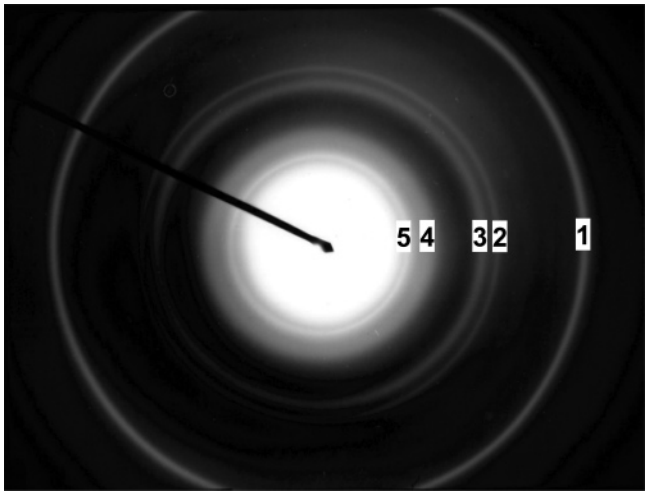

Figure 3. SAED pattern of Al−Si nanotubes. The numbers on the rings correspond to those in Table 1. The diffraction rings are due to the atomic periodicity within the nanotubes.

Table 1. *d*-Spacings of Rings Appearing in the SAED Pattern of Al−Si Nanotubes (Figure 3)[a]

reflection	*d* spacing (nm)	*hkl*	reflection	*d* spacing (nm)	*hkl*
1	0.14	006	4	0.32	071
2	0.21	004	5	0.43	002
3	0.22	063			

[a] The (*hkl*) indices are in the cylindrical C_{24h} space group. The (00*l*) reflections correspond to the periodic repeat unit along the nanotube axis.

III. Results and Discussion

III.1. Structure, Packing, and Composition of NTs. *III.1.1. TEM and SAED.* Figure 3 shows the SAED pattern of an Al−Si NT sample after 120 h of synthesis. Because the Al−Si and Al−Ge nanotubes are similar in molecular

(24) Horvath, G.; Kawazoe, K. *J. Chem. Eng. Jpn.* **1983**, *16* (6), 470−475.
(25) Saito, A.; Foley, H. C. *AIChE J.* **1991**, *37* (3), 429−436.
(26) Wyn, B. *Dynamic Light Scattering. The Method and Some Applications*; Clarendon Press: Oxford, 1993.

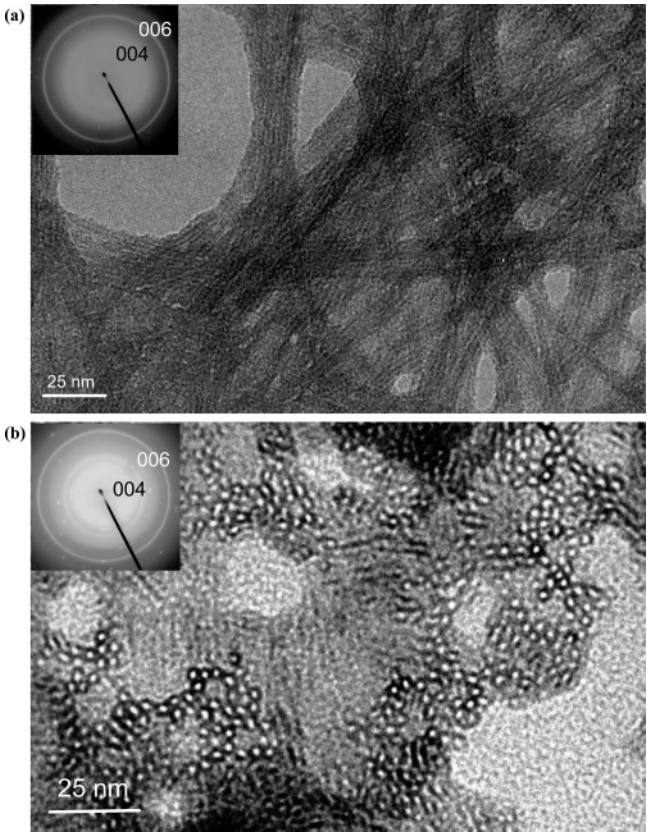

Figure 4. Transmission electron micrographs of (a) Al−Si and (b) Al−Ge nanotubes at a synthesis time of 120 h. The insets show SAED patterns obtained from the same samples.

structure, the ED patterns obtained were the same. The Miller indexed peaks and corresponding *d* spacings of the five most prominent rings in the ED pattern are tabulated in Table 1. The SAED patterns mainly probe the structure within the individual nanotubes and are important for tracking the formation of the nanotubes. With the crystallographic *c* axis along the nanotube axis, the (006) and (004) reflections occurring at *d* spacings of 0.14 and 0.21 nm are sharp and intense[7−9,12,13,27,28] and arise from the periodic unit cell of approximately 0.85 nm in the *c* direction. The diffraction spots due to the packing of the tubes are located very close to the central beam and can only be identified for very low selected areas (<20 μm) and low exposure times. The nanotube packing is better elucidated using XRD, as discussed later in this paper. As a result of the cylindrical (C_{24h}) symmetry of these nanotubes, the odd reflections along the *c* axis are absent. A similarly intense (006) reflection, as well as the (004) reflection, is observed for the Al−Ge nanotubes. The absence of the (003) or (005) reflections also supports the assignment of C_{24h} symmetry of the Al−Ge nanotubes. The (006) and (004) rings are, thus, taken as characteristic signatures that differentiate the nanotubes from any amorphous materials or other crystalline structures existing in the samples at various times during the reaction.

Figure 4a,b shows TEM micrographs of the Al−Si and Al−Ge nanotubes at a synthesis time of 120 h. The morphology of the Al−Si samples is that of bundles of close-packed nanotubes, the lengths of the bundles being close to 1 μm. The bundles form a random fibrous network. On the other hand, the Al−Ge nanotubes are much shorter, do not form any fibrous structures, and display a morphology consisting of nanotubes often standing upright on the surface of the polymeric TEM sample film. This distinct feature arising from the short length of the Al−Ge nanotubes enabled us to obtain clear TEM images down the axis of the Al−Ge nanotubes (Figure 4b). The diameters of the Al−Si and Al−Ge nanotubes appear to be highly monodisperse, being measured as 2.2 and 3.3 nm (outer diameter), respectively.

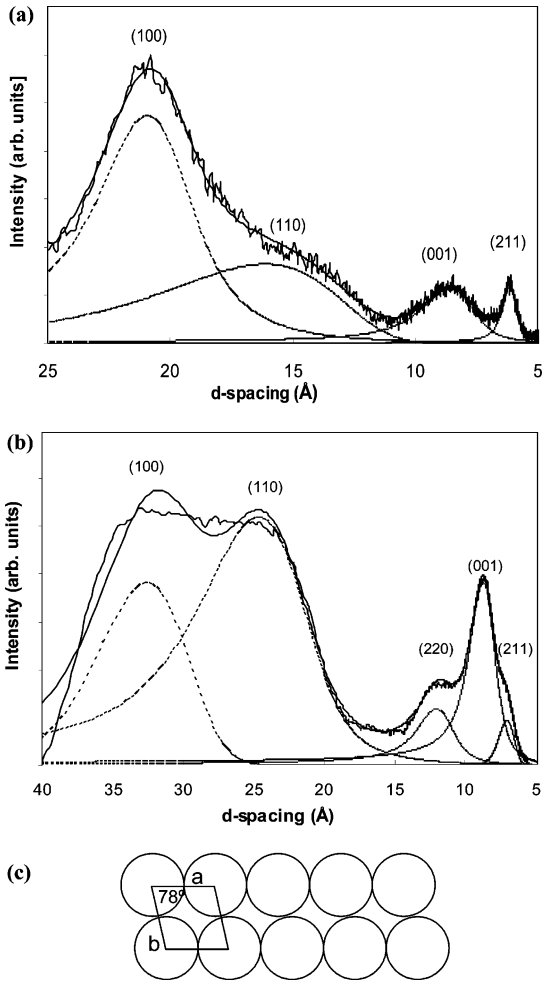

Figure 5. Grazing angle incidence XRD spectra from thin films of (a) Al−Si and (b) Al−Ge nanotubes obtained after 120 h of synthesis. The solid lines indicate the fitted spectra composed of a number of pseudo-Voigt peaks shown in the plots. (c) Monoclinic solid-state packing arrangement of the Al−Si and Al−Ge nanotubes.

III.1.2. XRD. Although XRD has been used in previous works to infer the presence of close-packed imogolite nanotubes, no analysis of the data in terms of the solid-state packing has been reported. We have analyzed the XRD patterns of the Al−Si and Al−Ge nanotubes, shown in parts a and b of Figure 5, respectively. First, the patterns were fitted by a combination of pseudo-Voigt line shapes, each corresponding to an (*hkl*) reflection. The fitted *d* spacings of the reflections are given in Table 2. In previous experimental and simulation studies, the packing of the nanotubes was assumed as hexagonal.[29] However, the appearance of XRD peaks at *d* spacings of 1.611 nm (Al−Si) and 2.467

(27) Barrett, S. M.; Budd, P. M.; Price, C. *Eur. Polym. J.* **1991**, *27* (7), 609−612.
(28) Farmer, V. C.; Adams, M. J.; Fraser, A. R.; Palmieri, F. *Clay Miner.* **1983**, *18* (4), 459−472.

Table 2. Miller Indices and *d*-Spacings of Bragg Reflections Obtained from the XRD Spectra of the Al−Si and Al−Ge Nanotubes[a]

Al−Si nanotubes[b]				Al−Ge nanotubes[c]			
h	*k*	*l*	*d* spacing (nm)	*h*	*k*	*l*	*d* spacing (nm)
1	0	0	2.105	1	0	0	3.253
1	1	0	1.672	1	1	0	2.585
0	0	1	0.851	2	2	0	1.292
2	1	1	0.656	0	0	1	0.851
				2	1	1	0.751

[a] The unit cells are monoclinic with dimensions as indicated. [b] Unit cell parameters: $a = b = 2.105$ nm, $c = 0.851$ nm; $\alpha = \beta = 90°$, $\gamma = 78°$. [c] Unit cell parameters: $a = b = 3.253$ nm, $c = 0.851$ nm; $\alpha = \beta = 90°$, $\gamma = 78°$.

nm (Al−Ge) cannot be explained by a hexagonal packing model. After considering all the possible unit cell types, it was found that only monoclinic unit cells could index the XRD patterns. Remarkably, the monoclinic angle (γ) was found to be exactly the same (78°) for both the Al−Si and the Al−Ge nanotubes (Figure 5c). Table 2 gives the unit cell dimensions and the Miller indices corresponding to all the fitted *d* spacings. The Al−Ge pattern shows five Bragg reflections assigned to the (001), (110), (001), (220), and (211) planes. However, the Al−Si XRD pattern shows four peaks with Bragg reflections at (001), (110), (001)/(220), and (211). Both the Al−Si and the Al−Ge nanotubes have the same aluminum hydroxide repeat unit of 0.851 nm along (001). The diameter of the Al−Si nanotube is such that the (001) and (220) reflections overlap indistinguishably; however, the two reflections are split in the Al−Ge nanotubes which retain the same repeat unit along (001) but have a larger diameter. Another feature arising from the XRD analysis is that the (001) planes of the individual nanotubes are apparently aligned with each other to produce an intense, though broad, (001) reflection from the overall packed structure. This deserves further study from the point of view of the interaction forces between the nanotubes that cause their condensation from solution into ordered mesostructures.

III.1.3. Nitrogen Adsorption. Figure 6a shows the nitrogen adsorption isotherms at 77 K for Al−Ge and Al−Si nanotubes (synthesized by a 120 h reaction, purified by dialysis, and outgassed at 250 °C for 12 h). The lower limit (10^{-3}) of the relative pressure (P/P_{sat}) was determined by the capability of the instrument to equilibrate at low pressures. Figure 6b shows the differential pore size distribution of the Al−Ge and Al−Si nanotubes. The pore size distribution was estimated using a modification for cylindrical pores[25,30] of the HK model.[24] The results agree very well with earlier adsorption studies on natural and synthetic imogolite[31] with the exception that no mesoporosity was observed in our samples. Both Al−Ge and Al−Si nanotubes show a narrow distribution of pore sizes centered at effective pore diameters of ∼0.9 and ∼0.65 nm, respectively. The pore size distributions are monomodal which strongly indicates a monodisperse diameter and an open-ended (uncapped) structure of the nanotubes. The diameter of the Al−Ge

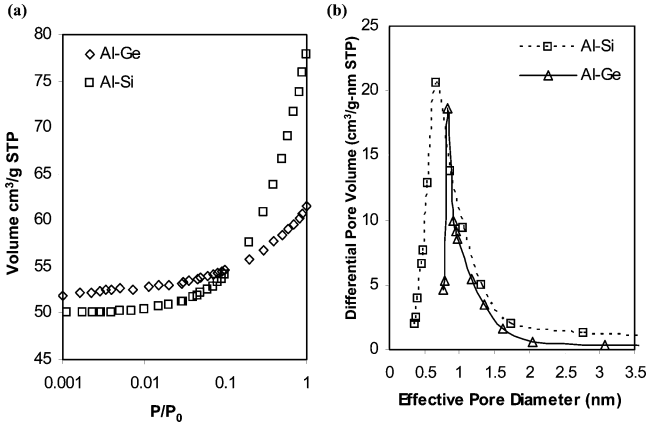

Figure 6. (a) Nitrogen adsorption isotherms at 77 K for freeze-dried Al−Si and Al−Ge nanotubes outgassed at 250 °C. (b) Differential pore size distributions of Al−Si and Al−Ge nanotubes obtained from nitrogen adsorption data shown in part a with the modified HK model for cylindrical pores.

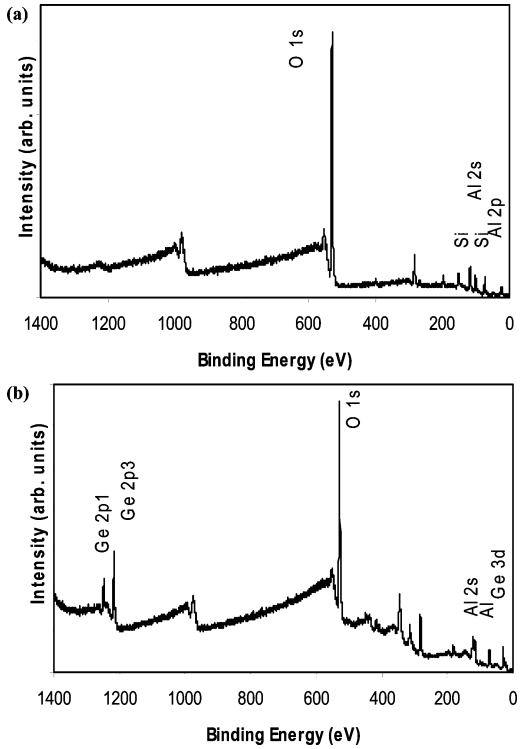

Figure 7. XPS survey spectra of thin films of (a) Al−Si and (b) Al−Ge nanotubes. The positions of the oxidation states of the elements are indicated.

nanotubes is substantially larger than that of Al−Si nanotubes. These conclusions are in agreement with TEM observations (section III.1.1). The effective pore diameters measured by nitrogen adsorption are lower than those visible by TEM. As argued by previous authors,[31] the exact values of the pore size should be taken with caution, being based on a number of assumptions regarding the pore geometry and the packing of nitrogen in the pores.[25,30]

III.1.4. XPS. XPS survey spectra for the Al−Si and the Al−Ge nanotube films are shown in parts a and b of Figure 7, respectively. The following photoelectron bands were used to calculate the composition of the sample: Al 2p (71.8 eV), Al 2s (116.79 eV), Ge $2p_{3/2}$ (1217.2 eV), Ge 3d (29.15 eV), Ge $2p_1$ (1220.7 eV), Si 2s (150.2 eV), and Si 2p (99.4 eV). The atomic concentrations obtained from fitting the peaks

(29) Tamura, K.; Kawamura, K. *J. Phys. Chem. B* **2002**, *106* (2), 271−278.
(30) Parent, M. A.; Moffat, J. B. *Langmuir* **1995**, *11* (11), 4474−4479.
(31) Ackerman, W. C.; Smith, D. M.; Huling, J. C.; Kim, Y. W.; Bailey, J. K.; Brinker, C. J. *Langmuir* **1993**, *9* (4), 1051−1057.

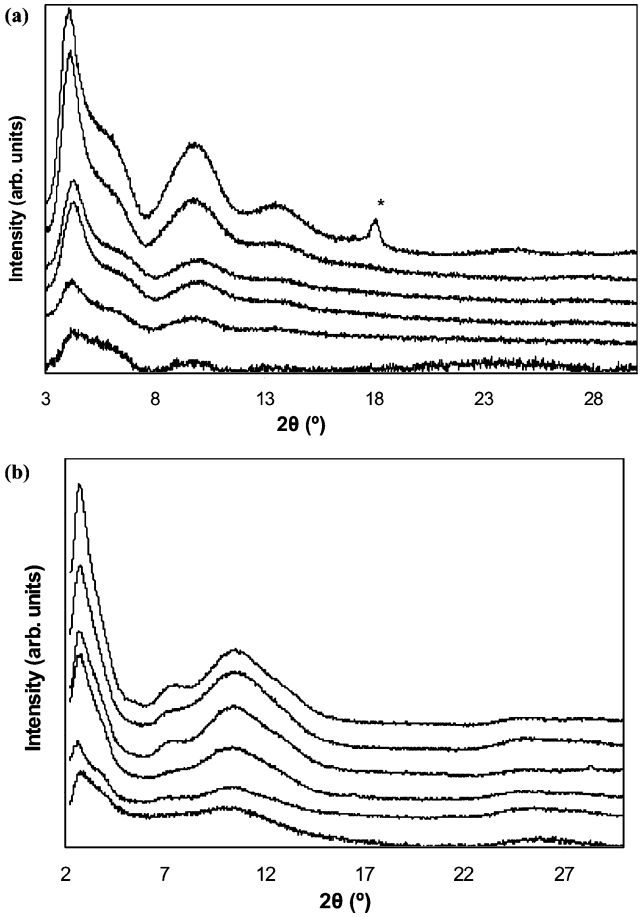

Figure 8. XRD spectra of (a) Al−Si and (b) Al−Ge nanotubes at synthesis times of 10, 24, 48, 72, 96, and 120 h, respectively, arranged from bottom to top with increasing synthesis time. The sharp peak (*) occurring in one of the samples is an unknown, nonreproducible impurity phase which is occasionally seen in XRD patterns from the synthesis products. The 10 h sample intensities have been increased by a factor of 2 from their original measured values for clarity.

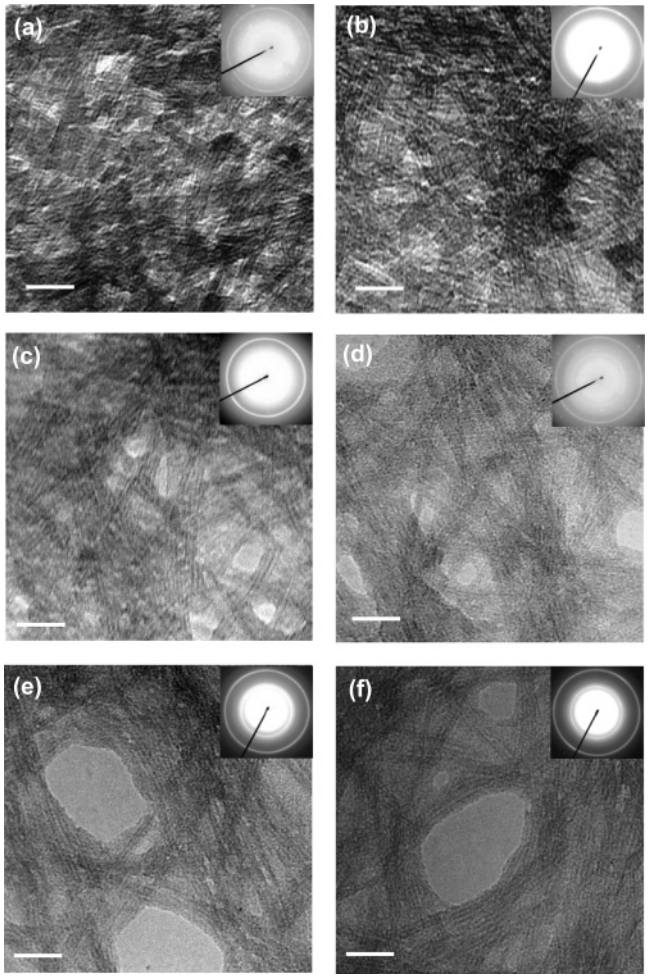

Figure 9. Transmission electron micrographs of Al−Si nanotubes as a function of synthesis time as indicated in the figures. The insets show the corresponding SAED patterns. The scale bar is 25 nm.

were 10.99% Al and 6.44% Si for the Al−Si nanotube film and 16.56% Al and 6.18% Ge for the Al−Ge nanotube film. The atomic concentration ratios (Al:X, X = Si or Ge) are, thus, close to 2, conforming to the expected chemical composition of the nanotubes.

III.2. Morphology Dependence on the Growth Time. *III.2.1. XRD.* Figure 8a,b shows the XRD patterns of Al−Si and Al−Ge nanotubes extracted from the reactor samples at reaction times of 10, 24, 48, 72, 96, and 120 h. It is apparent that all the peaks seen in the 120 h samples are clearly visible even at small reaction times (10 h). All the peaks increase in intensity as the reaction time is increased, showing clearly that the nanotubes are increasing in quantity, and indeed prefer the same solid-state packing arrangement throughout. Because the volume of sample dried on the glass slide was the same in all cases, the concentration of the nanotubes must be increasing with reaction time. The sharp peak appearing in the 120 h Al−Si sample (Figure 8a) is believed to originate from a dense impurity phase that occasionally forms in the synthesis product.

III.2.2. TEM and SAED. A series of TEM micrographs (Figure 9a−f) show the samples prepared directly from the Al−Si nanotube synthesis reactor at reaction times of 10, 24, 48, 72, 96, and 120 h, respectively. The SAED patterns are also inset in the figure. It is clear that nanotubes form as early as 10 h. This is inferred from the morphology of the TEM images and is well-supported by the occurrence of the (006) and (004) reflections in all the SAED patterns. Figure 10a−f shows the TEM micrographs of Al−Ge nanotubes at intermediate growth times of 10, 24, 48, 72, 96, and 120 h, and the insets show the SAED patterns. All the micrographs clearly show the presence of nanotubes from as early as 10 h and the reduction of amorphous materials with the increase in synthesis time. In the Al−Ge nanotube case, however, the nanotubes are relatively short (∼10 nm) as indicated before. Qualitative comparison of the images does not indicate any appreciable changes in the nanotube length and diameter or observable high polydispersity in either the length or the diameter.

III.3. Quantitative Analysis of Nanotube Growth by DLS. *III.3.1. Dynamic model.* DLS is a useful technique for studying the dimensions of nanoparticles in solution at dilute concentrations. The present synthesis produces micromolar concentrations of nanotubes in solution. This situation is ideal for DLS measurements but unfavorable for techniques such as small-angle X-ray scattering which require higher concentrations of nanoparticles to obtain quantitatively useful data. The characteristics of self-diffusion of rigid and flexible rodlike nanoparticles in dilute isotropic solutions have been

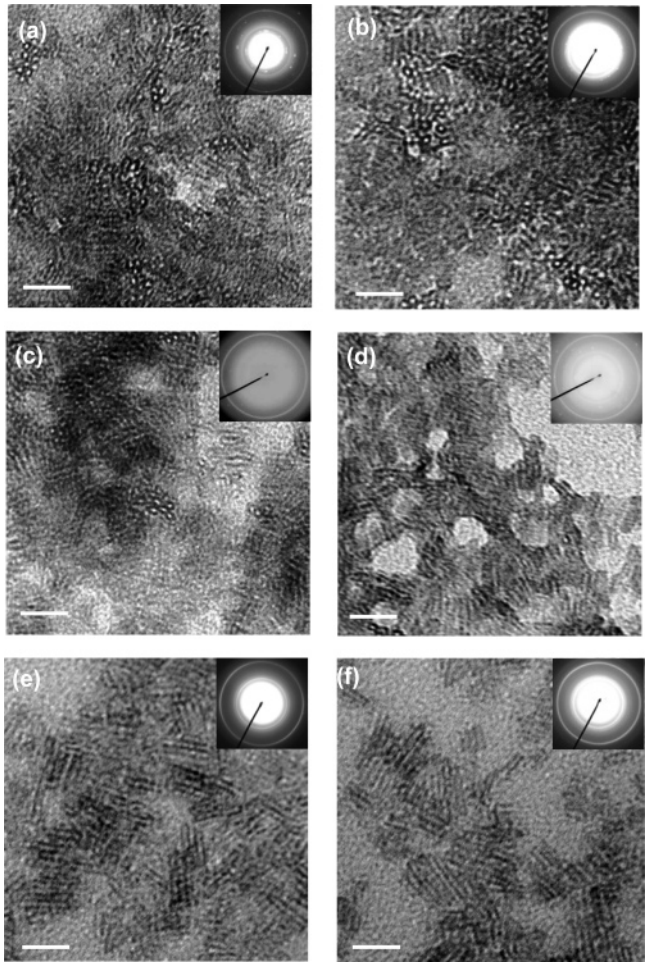

Figure 10. Transmission electron micrographs of Al−Ge nanotubes as a function of synthesis time as indicated in the figures. The insets show the corresponding SAED patterns. The scale bar is 25 nm.

the subject of extensive theoretical treatment[32−36] and have been used to fit DLS data and to determine the dimensions and polydispersity of rodlike nanoparticles such as viruses[37] and inorganic whiskers.[38] In this section we discuss briefly the theoretical details applicable to the system under investigation and then present the results of our DLS investigations into Al−Si and Al−Ge nanotube synthesis.

For a rigid rod nanoparticle undergoing Brownian translational and rotational motion in a solvent, the translational and rotational diffusivity coefficients D and Θ respectively are related as $L^2\Theta/D \sim 9$.[36] In particular, Θ has an L^{-3} dependence, where L is the length of the rod. When the rod length is short, the rotational diffusion becomes very rapid. If the time taken to rotationally circumscribe a sphere approaches the delay time ($\tau \sim 1\ \mu$s) of the autocorrelator, then the rapidly rotating rod can be approximated as a translationally diffusing sphere whose diameter equals the length of the rod. In our experiments the measured diffusion coefficients for the Al−Ge nanotubes were of the order of 5×10^{-7} cm^2/s, and the nanotube length as obtained from TEM micrographs was ~10 nm. Then $\Theta = 4.5 \times 10^6$ rad^2/s. The time taken to circumscribe a sphere is given as $2\pi^2/\Theta = 4.4\ \mu$s, which is close to the delay time of the autocorrelator. Thus, to the autocorrelator the rapidly rotating short rod is indistinguishable from a spherical nanoparticle whose diameter equals the length of the rod. Therefore, in the case of the short Al−Ge nanotubes, the length can be obtained in a simple manner from the diffusivity D via the Stokes−Einstein equation: $3\pi\eta_0 L/(kT) = D$. With an increase in the length of the rods (Al−Si nanotubes) the rotational motion becomes more sluggish and a full model for diffusion (described below) can be used for data analysis.

The Siegert equation[33] relates the normalized intensity autocorrelation function $g_2(t)$ with the field autocorrelation function $g_1(t)$ as $g_2(t) = 1 + \beta|g_1(t)|^2$. Here, β, the coherence factor,[33] is an adjustable parameter (taken as unity in dilute aqueous suspensions). The full model for the field autocorrelation function of a suspension of nanorods of uniform diameter but polydisperse length is[32,39,40]

$$g_1(t) = \int_0^\infty [a_0 \exp(-Q^2Dt + Q^4D^2t/120\Theta) + a_2 \exp(-Q^2Dt - 6\Theta t - Q^2Dt/7)]P(L)\,\mathrm{d}L \quad (1)$$

Here, Q is the momentum transfer given by $Q = (4\pi n/\lambda)\sin(\theta/2)$, where n is the refractive index of water, λ is the wavelength of the incident light, and θ is the scattering angle (90° in the present study). The function $P(L)$ is the distribution function of the rod lengths. The prefactors a_0 and a_2 are given as

$$a_0 = 1 - Q^2L^2/36 + 13Q^4L^4/32\,400 + Q^4L^2D/1080\Theta - Q^4D^2/720\Theta^2$$
$$a_2 = Q^4L^4/6480 - Q^4L^2D/1080\Theta + Q^4D^2/720\Theta^2 \quad (2)$$

This model can be used to obtain the nanotube length from DLS data, employing the expression for the translational diffusivity D of a slightly bending nanorod:[32,39,40]

$$\frac{3\pi\eta_0 LD}{kT} = \ln\left(\frac{L}{d}\right) + 0.3863 + 0.67(\chi L) + 0.018\,83(\chi L)^2 + \mathrm{O}(\chi L)^3 \quad (3)$$

Here, η_0 is the viscosity of the aqueous solvent (0.89 cP at 25 °C), χ is the inverse Kuhn length[41] which parametrizes the bending of the rods and which converges to zero for a perfectly rigid rod, L is the length of the rod, and d is the outer diameter. The observed signal intensity was in the region of 10 000−250 000 counts/s in all cases. The autocorrelator produces $g_2(t)$ with a high signal-to-noise ratio by means of repeated scans on the sample (see Experimental

(32) Yamakawa, H.; Fujii, M. *Macromolecules* **1973**, *6* (3), 407−415.
(33) Claire, K.; Pecora, R. *J. Phys. Chem. B* **1997**, *101* (5), 746−753.
(34) Aragon, S. R. *J. Chem. Phys.* **1980**, *73* (4), 1576−1580.
(35) Pecora, R. *J. Chem. Phys.* **1968**, *48* (9), 4126−4130.
(36) Phalakornkul, J. K.; Gast, A. P.; Pecora, R. *J. Chem. Phys.* **2000**, *112* (14), 6487−6494.
(37) Cush, R.; Dorman, D.; Russo, P. S. *Macromolecules* **2004**, *37* (25), 9577−9584.
(38) Lima, A. M. D.; Wong, J. T.; Paillet, M.; Borsali, R.; Pecora, R. *Langmuir* **2003**, *19* (1), 24−29.
(39) Donkai, N.; Inagaki, H.; Kajiwara, K.; Urakawa, H.; Schmidt, M. *Makromol. Chem.* **1985**, *186* (12), 2623−2638.
(40) Phalakornkul, J. K.; Gast, A. P.; Pecora, R. *Macromolecules* **1999**, *32* (9), 3122−3135.
(41) Yilgor, I.; Yurtsever, E.; Erman, B. *Macromolecules* **2002**, *35* (26), 9825−9831.

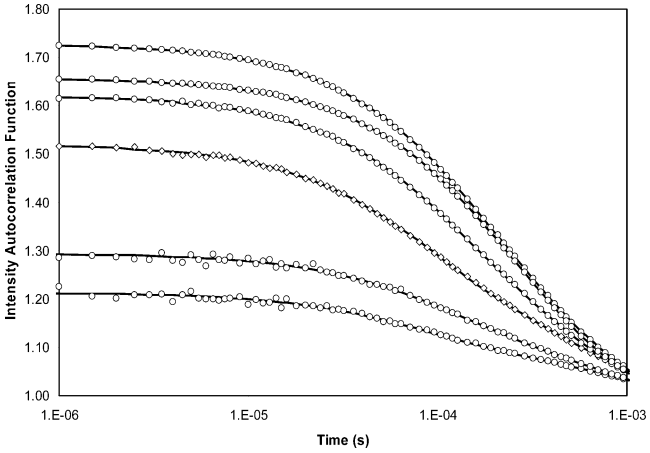

Figure 11. Photon intensity autocorrelation functions obtained from DLS measurements on Al−Si nanotube solutions at different synthesis times of 10, 24, 48, 72, 96, and 120 h, arranged from bottom to top with increase in synthesis time. The open circles are the measured data, and the solid lines are the calculated autocorrelation functions from the final values of the fitted structural parameters.

Section). Then $g_1(t)$ was obtained from $g_2(t)$ according to the Siegert relation, and the diffusion model (eqs 1−3) was directly fitted to $g_1(t)$ via a nonlinear least squares algorithm developed in-house. Initially, a monodisperse suspension was assumed. The only fit parameters are the nanotube length (L) and the inverse Kuhn length (χ). The diameter of the Al−Si nanotubes was taken as $d = 2.2$ nm on the basis of the TEM images. The values of the nanotube length were used in a subsequent fit incorporating a length distribution function $P(L)$ of Gaussian form, that is, $P(L) = \{1/[(2\pi)^{1/2}\sigma_L]\} \exp[-(L - \bar{L})^2/2\sigma_L{}^2]$.

III.3.2. Results. Examples of the nonlinear least-squares fits of the measured $g_2(t)$ data are shown in Figure 11. The open circles are the experimental autocorrelation functions of samples taken at different synthesis times, and the solid lines correspond to the calculated autocorrelation functions using the final values of the fitted parameters. The fits are of excellent quality, and the residuals are less than 1%. For the case of the Al−Si nanotubes where the inverse Kuhn length (χ) was included as a fitting parameter, it was found that this parameter always converged to zero; that is, the nanotubes behave as rigid rods in solution. This coincides with a result from previous work which used natural imogolite fibers dispersed in water,[39] wherein no bending effects of the Al−Si nanotubes were observed. In the case of the Al−Ge nanotubes, no bending effects are expected at all, owing to their extremely short lengths. Finally, the inclusion of the Gaussian distribution of lengths (to describe polydispersity) resulted in no appreciable standard deviation in the nanotube lengths. The fitted standard deviations are in the range of 0−1 nm, which are not statistically significant. Hence, the nanotubes are regarded as monodisperse in length, to the limits of DLS measurement from nanoparticles.[42]

The fitted lengths of the nanotubes as functions of synthesis time are shown in Figure 12, for both Al−Si and Al−Ge nanotubes. The error bars on the fitted lengths are obtained by averaging the results from four independent samples taken in different experiments. An important result

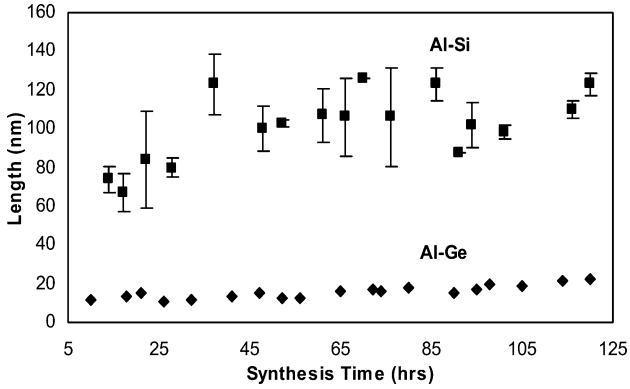

Figure 12. Fitted lengths of Al−Si and Al−Ge nanotubes obtained from DLS experiments, as a function of synthesis time from 10 to 120 h.

of this analysis is that the nanotubes do not grow in length substantially as a function of synthesis time. Considering the error bars on the data, there does not appear a physically significant "growth rate" for the nanotube lengths. Small increases, if any, in the fitted lengths could also be due to some aggregation of the nanotubes at higher concentrations. The Al−Si nanotubes average about 100 nm in length, whereas the Al−Ge nanotubes are about 15 nm in length. These results are well-consistent with the detailed TEM observations.

The practically constant length of the nanotubes throughout the synthesis time (of over 100 hrs) appears to favor a self-assembly mechanism, over a kinetic mechanism involving the formation of "proto-nanotube" intermediates which increase in length by addition of precursors. The samples, after filtration through a 0.2 μm filter, do not reveal any other significant population of nanoparticles except for the nanotubes themselves. This indicates that the nutrient sources for nanotube formation are either sub-nanometer aluminosilicate oligomers which cannot be detected by DLS or a few large gel-like particles suspended in solution and which are removed by filtration. The former possibility is also consistent with NMR spectroscopic studies of acidic gibbsite-forming aluminum(III) hydroxide solutions, wherein no oligomeric precursors other than the monomer and the dimer have been conclusively established.[43] It should be noted that acidic aluminosilicate solutions, with aluminum in primarily octahedral coordination,[43,44] are completely different at a molecular level from the large variety of precursors seen in alkaline solutions.[45] In addition, the highly dilute solutions used here may favor only the formation of a small number of oligomeric precursors. While none of the techniques can provide conclusive evidence regarding the polydispersity of the nanotube length, the DLS fit results and the presence of a well-ordered solid-state structure, as well as qualitative observation of the TEM images, do not support a high polydispersity in nanotube length.

In light of the present work, it is suggested that the nanotubes are the product of a thermodynamically controlled

(42) Sauer, T.; Wegner, G. *Macromolecules* **1991**, *24* (9), 2240−2252.
(43) Faust, B. C.; Labiosa, W. B.; Dai, K. H.; Macfall, J. S.; Browne, B. A.; Ribeiro, A. A.; Righter, D. D. *Geochim. Cosmochim. Acta* **1995**, *59* (13), 2651−2661.
(44) Exley, C.; Schneider, C.; Doucet, F. J. *Coord. Chem. Rev.* **2002**, *228* (2), 127−135.
(45) Swaddle, T. W. *Coord. Chem. Rev.* **2001**, *219*, 665−686.

molecular self-assembly process. In other words, the formation of a small (10−100 nm in length) nanotubular molecule of monodisperse diameter is the final step or the termination of the reaction rather than a nucleation step for the growth of longer nanotubes. In this case, control over the nanotube dimensions is unlikely to be obtained by increasing the synthesis time or adding reactants continuously to the synthesis reactor in the hope of extending the nanotube length but rather by thermodynamic control over the reaction chemistry. For example, the substitution of silicon with germanium leads to a substantial, yet precise and reproducible, change in the nanotube diameter and length. Other possible methods of thermodynamic control include the use of organosilane precursors (which contain a Si−C bond). These could potentially lead to the formation of well-defined nanotubes with organic-functionalized interiors. From the viewpoint of technological applications, the prevalence of thermodynamic control has advantages in terms of the ability to obtain nanotubes whose dimensions are governed more precisely by the thermodynamics of the self-assembly process. The 10 and 100 nm nanotubes can be regarded as nanocomponents that should be well-amenable to applications in areas as diverse as nanocomposites and nanobiotechnology. The above synthetic and mechanistic issues, as well as applications of the Al−Si and Al−Ge nanotubes, are under detailed investigation in our laboratory.

IV. Conclusion

The phenomenology of formation of single-walled aluminosilicate and aluminogermanate nanotubes has been examined by a combination of characterization techniques (TEM, SAED, XRD, XPS, N_2 adsorption, and DLS) to probe the nanotube structure, composition, packing, and dimensions as a function of synthesis time. By TEM and DLS analysis, it is found that the dimensions of the aluminogermanate nanotubes are 3.3 nm in diameter and approximately 15 nm in length, whereas those of the aluminosilicate nanotubes are 2.2 nm and approximately 100 nm, respectively. The Al/Si and Al/Ge atomic ratios are found to be 1.71 and 2.68, respectively, by XPS analysis, consistent with the accepted structural model of these nanotubes. Nitrogen adsorption clearly shows the monodisperse diameter of the nanotubes. The combined TEM, SAED, and XRD data show clearly that nanotube materials are formed at an early stage in the reaction and that the structure of the nanotubes remains essentially identical throughout the synthesis. However, the nanotube concentration increases with synthesis time. XRD analysis shows that their solid-state packing is well-ordered in an apparently monoclinic, and not hexagonal, arrangement. Furthermore, the synthetic nanotubes are individually dispersed in an acidic aqueous solution, allowing quantitative analysis of their dimensions by DLS. The present evidence strongly indicates that their dimensions (both length and diameter) do not change significantly with synthesis time. The sum total of the experimental data lends substance to our proposal that self-assembly thermodynamics of the aluminosilicate precursor solution, rather than kinetic (inorganic nucleation and growth) processes, exert control over the nanotube formation. In addition, the confirmation of well-defined, uncapped, hydrophilic, dispersible, synthetic nanotube materials is of significance for a number of potential nanotechnological applications.

Acknowledgment. The authors acknowledge financial support from the Georgia Institute of Technology through research start-up funding. V.M.B. acknowledges additional support from Georgia Tech through a President's Undergraduate Research Award (PURA) grant.

CM0505852